Supporting information

Hemin-Based Conjugated Effect Synthesis of Fe-N/NCNT Catalysts for Enhanced Oxygen Reduction

Yue Lu[a], Han Zhang [a]*, Shaojun Liu[a], Chenglong Li[a], Lixiang Li[a], Baigang An[a] and Chengguo Sun[a, b,]*

[a] School of Chemical Engineering, University of Science and Technology Liaoning, Anshan 114051, China

[b] School of Chemical Engineering, Nanjing University of Science and Technology, Xiaolingwei 200, Nanjing, Jiangsu 210094, China

* Correspondence and requests for materials should be addressed to C. Sun (email: cgsun@njust.edu.cn) and H. zhang (email: hzhang0807@163.com)

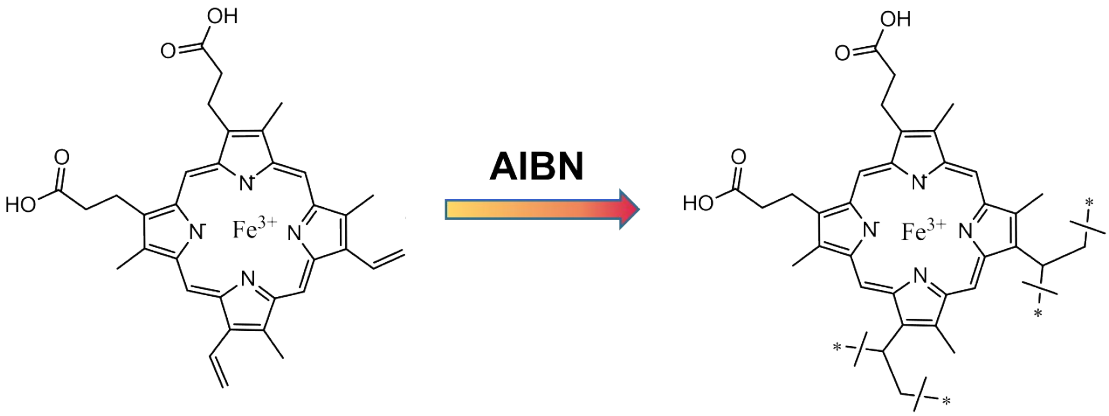

Figure S1. The synthetic pathway to synthesize the network structure.

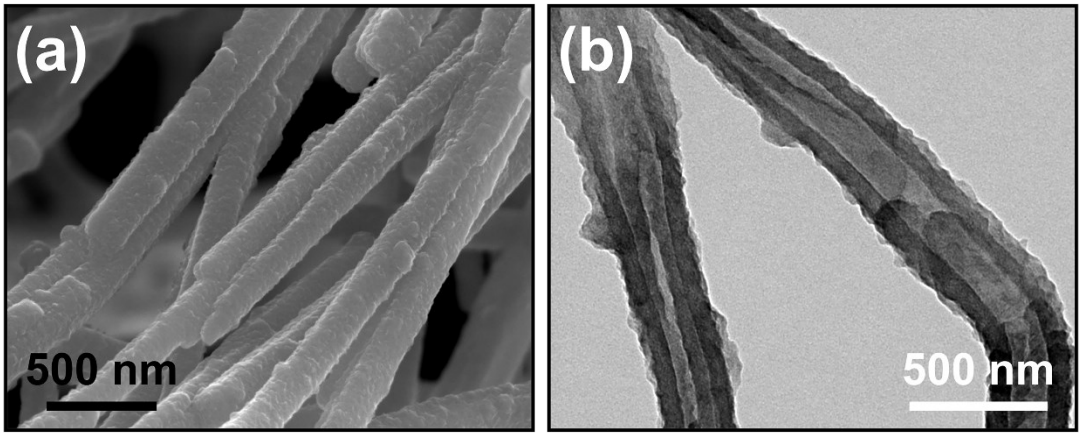

Figure S2. (a) SEM and (b) TEM images of polypyrrole nanotubes (PPy).

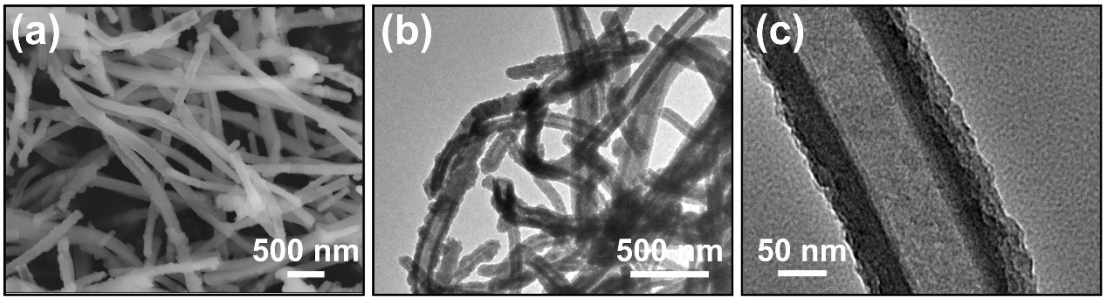

Figure S3. (a) SEM and (b, c) TEM images of A-PPy.

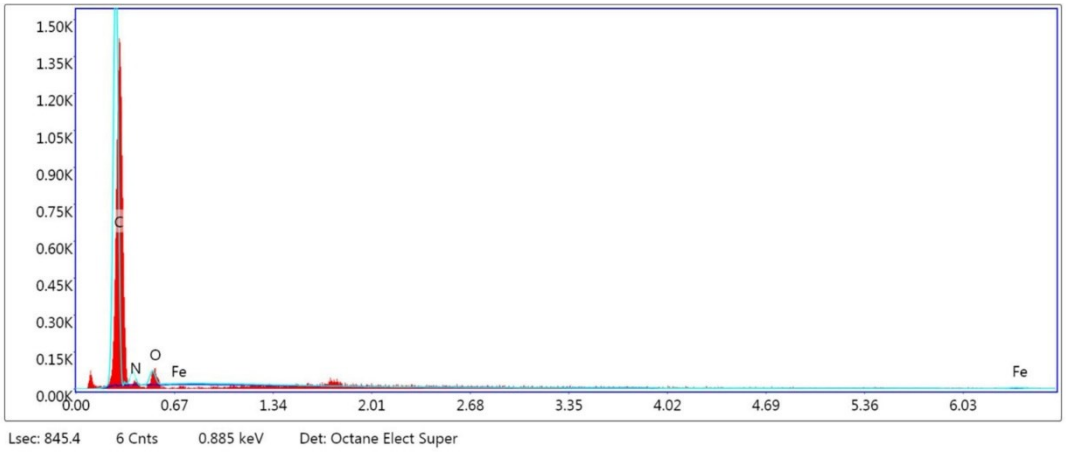

Figure S4. EDS spectrum of the Fe-NCNT-800.

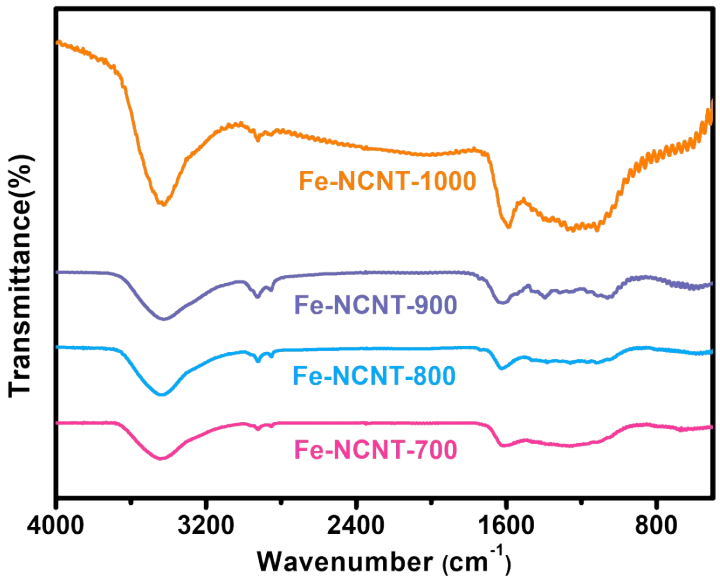

Figure S5. The FT-IR spectrum of Fe-NCNT-X (700-100) catalysts.

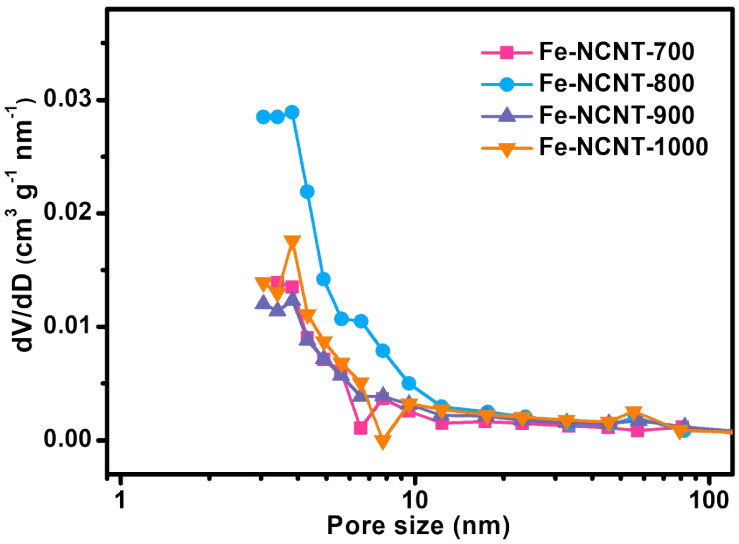

Figure S6. N_2 adsorption-desorption isotherm of Fe-NCNT-X (700-1000) and the corresponding pore size distribution of the BJH method.

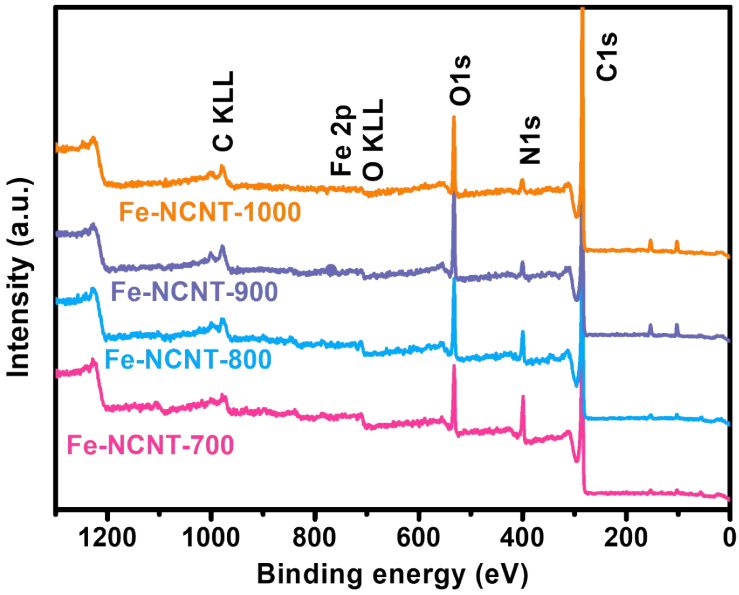

Figure S7. XPS survey spectra of Fe-NCNT-X (700-1000) catalysts.

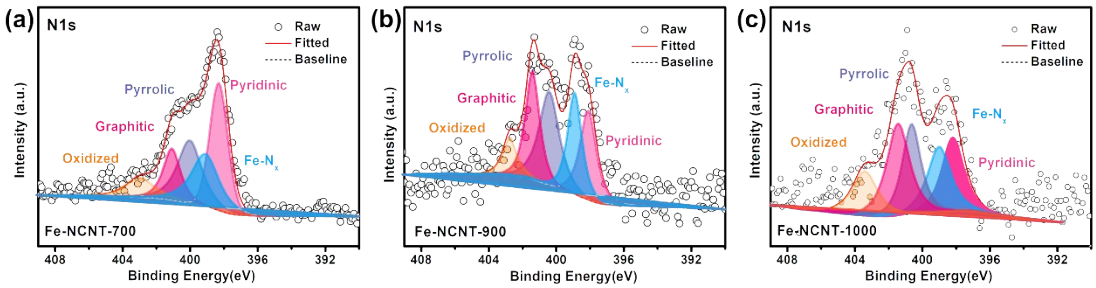

Figure S8. High-resolution XPS spectroscopy of N 1s of (a) Fe-NCNT-700, (b) Fe-NCNT-900 and (c) Fe-NCNT-1000.

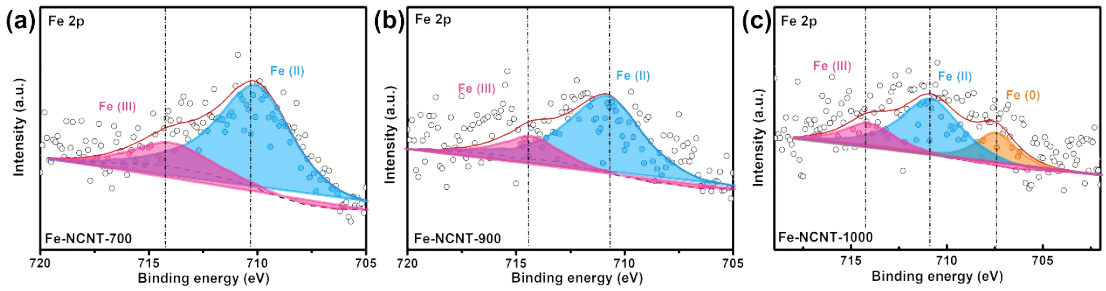

Figure S9. High-resolution XPS spectroscopy of Fe 2p of (a) Fe-NCNT-700, (b) Fe-NCNT-900 and (c) Fe-NCNT-1000.

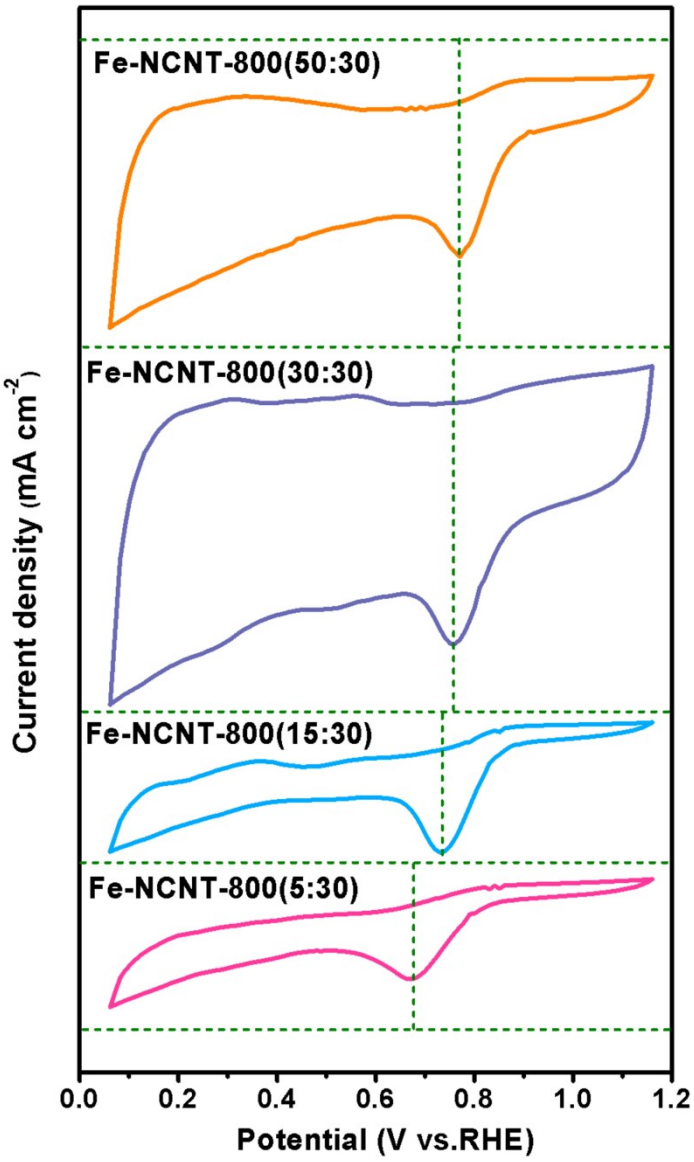

Figure S10. Cyclic voltammetry (CV) curves of Fe-NCNT synthesized at different ratios (mass ratio).

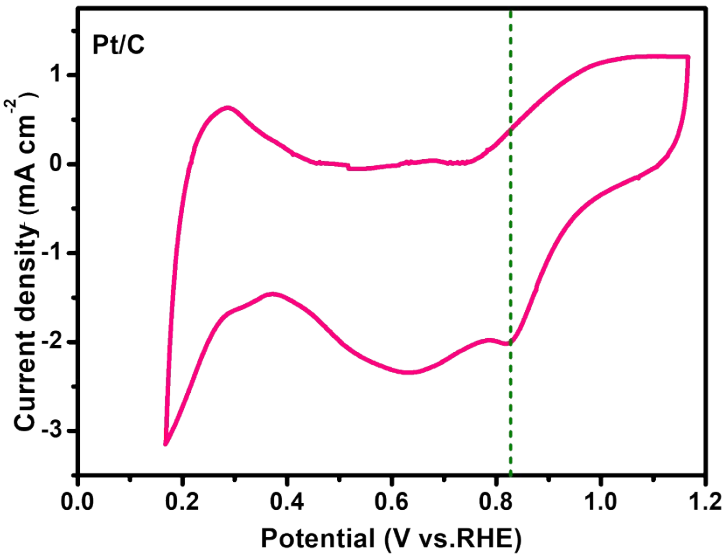

Figure S11. CV curve of Pt/C in O_2-saturated 0.1 M KOH at a scan rate of 50 mV s^{-1}.

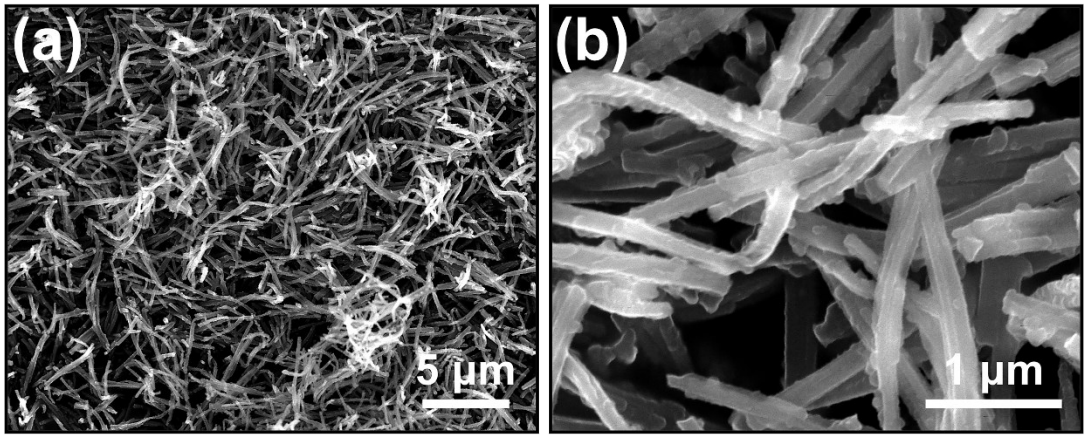

Figure S12. (a, b) SEM images of NCNT-800.

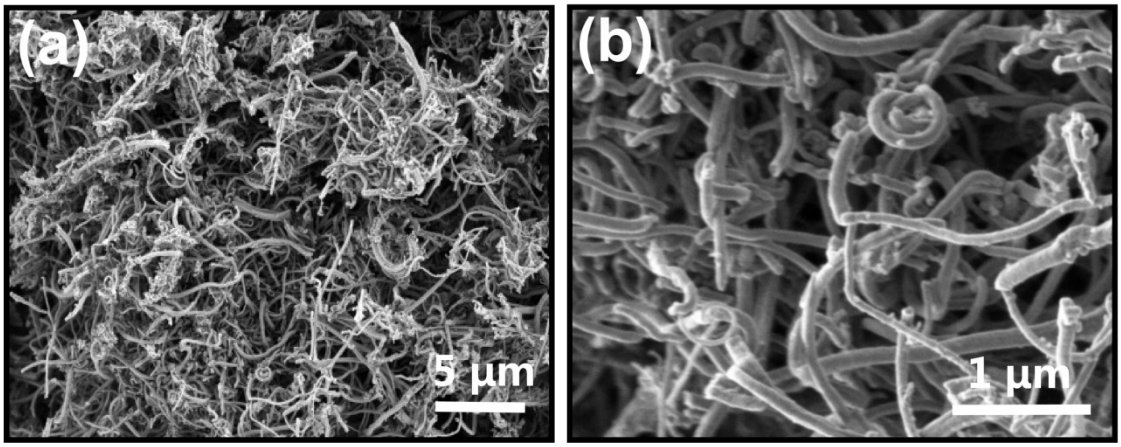

Figure S13. (a, b) SEM images of C-Fe-NCNT-800.

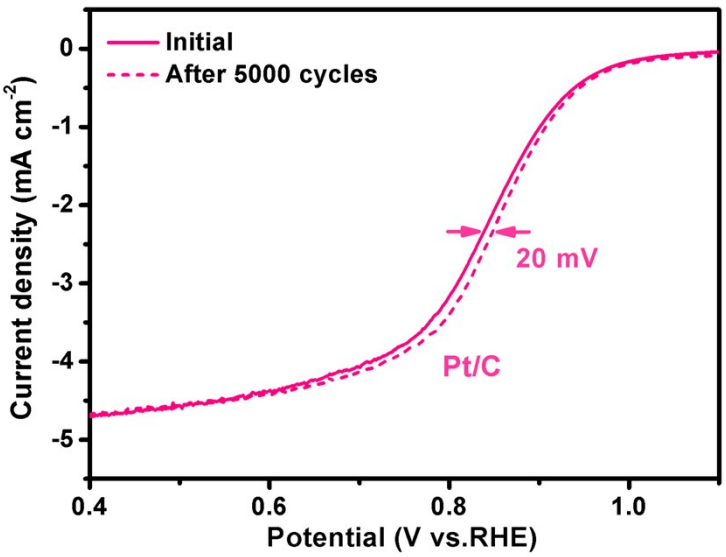

Figure S14. LSV before and after a 5000-cycle ADT of ORR on Pt/C in O_2-saturated 0.1 M KOH.

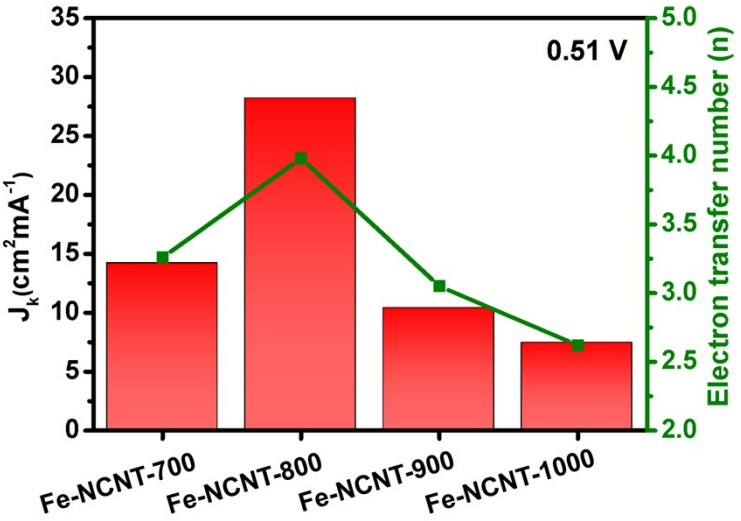

Figure S15. The kinetic current density (J_k) at 0.51 V and the number of electron transfer n value of Fe-NCNT-X (X=700-1000).

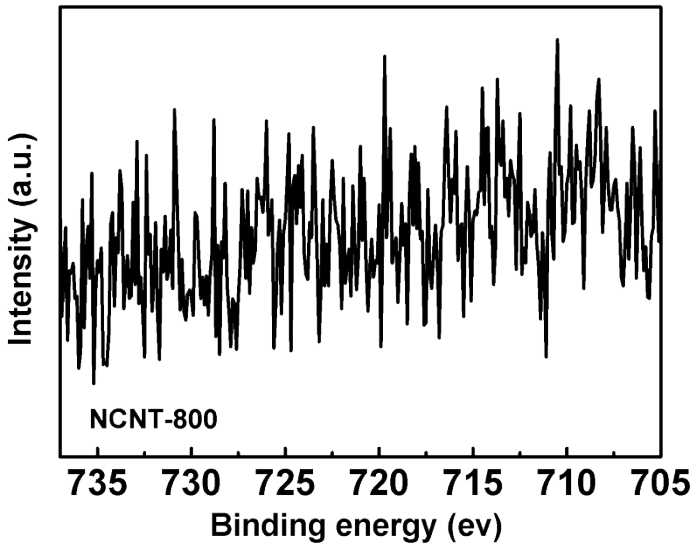

Figure S16. High-resolution XPS spectroscopy of Fe 2p electrons of NCNT-800.

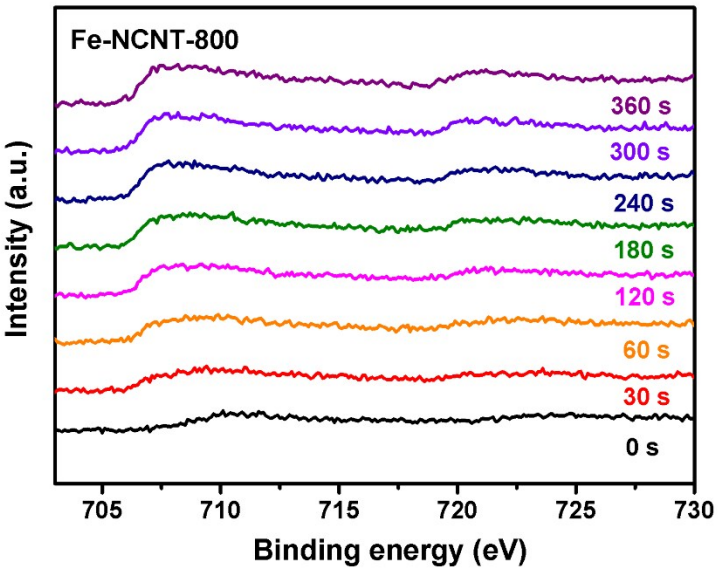

Figure S17. High-resolution XPS spectra of Fe 2p electrons with different Ar plasma etching times for Fe-NCNT-800 samples.

Table S1. Summary of surface properties of Fe-NCNT-X (700-1000) catalysts obtained from BET.

Sample	BET surface area ($m^2 g^{-1}$)	Pore size (nm)	Pore volume ($cm^3 g^{-1}$)
A-PPy	39.80	11.34	0.1129
Fe-NCNT-700	52.46	3.826	0. 1894
Fe-NCNT-800	104.2	3.825	0.2865
Fe-NCNT-900	48.66	3.832	0.2351
Fe-NCNT-1000	55.20	3.832	0.2451

Table S2. The relative content of different N sites obtained by high resolution XPS scanning of N1s.

Sample	Pyridinc N (%)	Fe-N (%)	Pyrrolic N(%)	Graphitc N(%)	Oxidized N(%)
Fe-NCNT-700	32.7	21.7	24.8	13.3	8.3
Fe-NCNT-800	28.0	28.5	27.4	10.2	5.9
Fe-NCNT-900	21.4	21.2	27.4	22.4	7.6
Fe-NCNT-1000	19.8	18.7	20.9	26.4	14.2

Table S3. The relative content of different Fe sites obtained by high resolution XPS scanning of Fe 2p.

Sample	Fe(0)(%)	Fe(II)(%)	Fe(III)(%)
Fe-NCNT-700	--	81.57	18.43
Fe-NCNT-800	--	87.06	12.94
Fe-NCNT-900	--	82.78	17.22
Fe-NCNT-1000	24.11	57.50	18.39

Table S4. The depth XPS spectra of N 1s with different Ar plasma etching times for Fe-NCNT-800.

Fe-NCNT-800	Pyridinic N(%)	Fe-N_x(%)	Pyrrolic N(%)	Graphitic N(%)	Oxidized N(%)
0 s	28.0	28.5	27.4	10.2	5.9
60 s	25.8	25.4	30.4	11.3	7.1

Table S5. Summary of LSV data for Fe-NCNT catalysts prepared in different synthesis ratios (mass ratio).

Sample	E_{onset}(V vs RHE)	$E_{1/2}$（V vs RHE）	J(mA cm^{-2})
Fe-NCNT-800(5:30)	0.89	0.66	-2.86
Fe-NCNT-800(15:30)	0.91	0.73	-4.02
Fe-NCNT-800(30:30)	0.93	0.79	-5.02
Fe-NCNT-800(50:30)	0.93	0.76	-4.36
Pt/C	1.06	0.82	-4.64

Table S6. Summary of LSV data for Fe-NCNT-X (X=700-1000) catalyst, NCNT-800, C-Fe-NCNT-800 and Pt/C.

	E_{onset} (V vs.RHE)	$E_{1/2}$ (V vs.RHE)	J (mA cm^{-2})
Fe-NCNT-700	0.90	0.72	-3.85
Fe-NCNT-800	0.93	0.79	-5.02
Fe-NCNT-900	0.89	0.71	-3.82
Fe-NCNT-1000	0.81	0.62	-3.2
Pt/C	1.06	0.82	-4.64
NCNT-800	0.82	0.66	-3.53
C-Fe-NCNT-800	0.87	0.75	-2.49

Table S7. The element summary table of high resolution XPS for different times of Ar plasma etching of Fe-NCNT-800 sample.

Times	C Atomic（%）	N Atomic（%）	O Atomic（%）	Fe Atomic（%）
0s	82.46	7.17	9.65	0.72
30s	87.97	6.58	4.57	0.88
60s	89.24	6.92	3.10	0.74
120s	89.14	6.72	2.90	1.23
180s	88.91	7.22	2.48	1.39
240s	90.25	6.41	2.29	1.05
300s	89.71	6.45	2.54	1.30
360s	89.16	7.43	2.15	1.26

Table S8. Comparison of ORR performance of Fe-NCNT-800 and other porphyrin-derived electrocatalysts and hollow structures.

Electrocatalysts	$E_{1/2}$ (V vs.RHE)	E_{onset} (V vs.RHE)	Electrolyte	Reference
Fe-NCNT-800	**0.79**	**0.93**	**0.1 M KOH**	**This work**
p-Fe-N-CNFs	0.82	0.91	0.1 M KOH	[1]
CoP-CMP800	0.79	0.84	0.1 M KOH	[2]
rGO/(Ni^{2+}/THPP/Co^{2+}/THPP)	0.71	0.84	0.1 M KOH	[3]
FNCT800-100	0.82	0.93	0.1 M KOH	[4]
Fe-N-C/HPC-NH_3	0.803	0.945	0.1 M KOH	[5]
Fe-N-C	0.72	0.83	0.5 M H_2SO_4	[6]
Fe-N-C/H_2O_2	0.79	0.93	0.1M$HClO_4$	[7]
Fe-N-C / MXene	0.84	0.92	0.1 M KOH	[8]
C60-SWCNT5	0.82	0.88	0.1 M KOH	[9]
H-Mn_3O_4-TMSLs	0.84	0.91	0.1 M KOH	[10]
HT-NCT	0.76	0.89	0.1 M KOH	[11]
Mo_2C/NPCNFs	0.77	0.90	0.1 M KOH	[12]
Co–N–GN	0.80	0.87	0.1 M KOH	[13]
TPA-TPE-2	—	0.82	0.1 M KOH	[14]
rGO/(Ni^{2+}/THPP/Co^{2+}/THPP)	0.71	0.84	0.1 M KOH	[15]

Reference

[1] Hu B, Wu Z, Chu S, et al. SiO_2-protected shell mediated templating synthesis of Fe–N-doped carbon nanofibers and their enhanced oxygen reduction reaction performance[J]. Energy and Environmental Science, 2018, 11(8): 2208-2215.

[2] Wu Z, Chen L, Liu J, et al. High-Performance Electrocatalysts for Oxygen Reduction Derived from Cobalt Porphyrin-Based Conjugated Mesoporous Polymers[J]. Advanced Materials, 2014, 26(9): 1450-1455.

[3] Sun J, Yin H, Liu P, et al. Molecular engineering of Ni–/Co–porphyrin multilayers on reduced graphene oxide sheets as bifunctional catalysts for oxygen evolution and oxygen reduction reactions[J]. Chemical Science, 2016, 7(9): 5640-5646.

[4] Tang F, Lei H, Wang S, et al. A novel Fe–N–C catalyst for efficient oxygen reduction reaction based on polydopamine nanotubes[J]. Nanoscale, 2017, 9(44): 17364-17370.

[5] Liu X, Liu H, Chen C, et al. Fe_2N nanoparticles boosting FeN_x moieties for highly efficient oxygen reduction reaction in Fe-N-C porous catalyst[J]. Nano Research, 2019, 12:1651–1657.

[6] Osmieri L, Escudero-Cid R, Monteverde Videla A H A, et al. Performance of a Fe-N-C catalyst for the oxygen reduction reaction in direct methanol fuel cell: Cathode formulation optimization and short-term durability[J]. Applied Catalysis B Environmental, 2017, 201:253-265.

[7] Wei X, Luo X, Wang H, et al. Highly-defective Fe-N-C catalysts towards pH-Universal oxygen reduction reaction[J]. Applied Catalysis B-environmental, 2019, 263:118347.

[8] Jiang L, Duan J, Zhu J, et al. Iron-Cluster-Directed Synthesis of 2D/2D Fe–N–C/MXene Superlattice-like Heterostructure with Enhanced Oxygen Reduction Electrocatalysis[J]. ACS Nano, 2020, 14(2):2436-2444.

[9] Gao R, Dai Q, Du F, et al. C(60)-Adsorbed Single-Walled Carbon Nanotubes as Metal-Free, pH-Universal, and Multifunctional Catalysts for Oxygen Reduction, Oxygen Evolution, and Hydrogen Evolution[J]. Journal of the American Chemical Society, 2019, 141(29):11658-11666.

[10] Li T, Xue B, Wang B, et al. Tubular Monolayer Superlattices of Hollow Mn_3O_4 Nanocrystals and Their Oxygen Reduction Activity[J]. Journal of the American Chemical Society, 2017, 139(35):12133-12136.

[11] Wei W, Ge H, Huang L, et al. Hierarchically Tubular Nitrogen-doped Carbon Structures for Oxygen Reduction Reaction[J]. Journal Materials of Chemistry A, 2017, 5(26):13634-13638.

[12] Wang H, Sun C, Cao Y, et al. Molybdenum carbide nanoparticles embedded in nitrogen-doped porous carbon nanofibers as a dual catalyst for hydrogen evolution and oxygen reduction reactions[J]. Carbon, 2017, 114(Complete):628-634.

[13] Jiang S, Zhu C, Dong S. Cobalt and nitrogen-cofunctionalized graphene as a durable non-precious metal catalyst with enhanced ORR activity[J]. Journal of Materials Chemistry A, 2013, 1(11):3593.

[14] Roy S, Bandyopadhyay A, Das M, et al. Redox-active and Semi-conducting Donor-Acceptor Conjugated Microporous Polymers as Metal-free ORR Catalysts[J]. Journal of Materials Chemistry A, 2018, 6(14):5587-5591.

[15] Sun J, Huajie Y, Liu P, et al. Molecular Engineering of Ni-/Co-Porphyrin Multilayers on Reduced Graphene Oxide Sheets as Bifunctional Catalysts for Oxygen Evolution and Oxygen Reduction Reactions[J]. Chemical Science, 2016, 7(9):5640-5646.